Analysis and Modeling of a Piezoelectric Transformer in High Output Voltage Applications

Gregory Ivensky, Moshe Shvartsas, and Sam Ben-Yaakov*

Power Electronics Laboratory
Department of Electrical and Computer Engineering
Ben-Gurion University of the Negev
P. O. Box 653, Beer-Sheva 84105
ISRAEL

Tel: +972-7-646-1561; Fax: +972-7-647-2949
Email: sby@ee.bgu.ac.il.
Web site: http://www.ee.bgu.ac.il/~pel

***Abstract*-Piezoelectric transformers (PZT) can be used advantageously in high output voltage DC-DC converters. In such applications the output section includes a voltage doubling rectification scheme to help increase the output voltage. This topology was modeled and analyzed by considering the expected voltage and current waveforms under the first harmonics approximation. The results were then used to build a linear AC equivalent circuit that emulates the AC-DC stage. The proposed model was verified against experimental results.**

I. INTRODUCTION

Piezoelectric transformers (PZT) were shown to be advantageous in DC-DC converter applications and in Cold Cathode Fluorescent Lamps (CCFL) drivers [1-7]. The favorable attributes of the PZT are: low weight and size and potentially low cost. One additional important characteristic is the high voltage isolation of the ceramic materials used to build PZTs. This advantage is especially important when the PZT is applied in High output Voltage (HV) applications. In these cases, the inherent high voltage isolation eliminates the relatively larger size and higher production costs normally associated with high voltage electromagnetic transformers.

In HV converters, one would like to avoid the use of output filter inductors which become bulky and highly expensive under the HV operating conditions. The classical alternative is the capacitor filter that is more practical under high output voltage - and hence relatively lower current - conditions. It has been documented that in this operating scheme, the output voltage and the resonant frequency of the PZT are highly dependent on the load, but no systematic analysis has been presented hitherto to examine these relationships.

In this study we develop a model of the PZT operating in HV applications and apply the model to derive analytical expressions that describe the interdependence of key parameters. These are then used to develop an AC equivalent circuit that emulates the behavior of the PZT based HV AC-DC stage.

II. THE PZT AND RECTIFIER

The conventional equivalent circuit of the PT includes (Fig. 1a): an ideal transformer T with turn ratio n, an input capacitor C_{in}, an output capacitor C_o and a series branch $R_m L_r C_r$ which represents mechanical resonance at the frequency

$$f_r = \frac{1}{2\pi\sqrt{L_r C_r}} \qquad (1)$$

and losses (emulated by R_m).

The equivalent circuit of Fig. 1a is erroneous since it allows a DC path through the secondary of the transformer used to emulate the mechanical gain. This path does not exist in the physical PZT. In the case of the voltage doubler scheme, to be considered here, one expect a DC voltage to be built across C_o which will be inconsistent with the electromagnetic transformer presentation. Furthermore, the transformer in the model of Fig. 1a is assumed to be ideal namely, having infinitely large magnetization inductance. This may pose some problems when applying the model in SPICE simulation (long stabilization time and lack of convergence). To remedy these, we propose the improved model of Fig. 1b. In this model, the action of the ideal transformer is emulated by two current dependent sources: a voltage source at the primary and a current source at the secondary. The turns ratio appears now as the gain factor of these sources. A clear advantage of the proposed model is that it does not introduce inductive components when used in SPICE simulation. A second advantage is that it allows DC components as does the physical PZT. The DC component

* Corresponding author

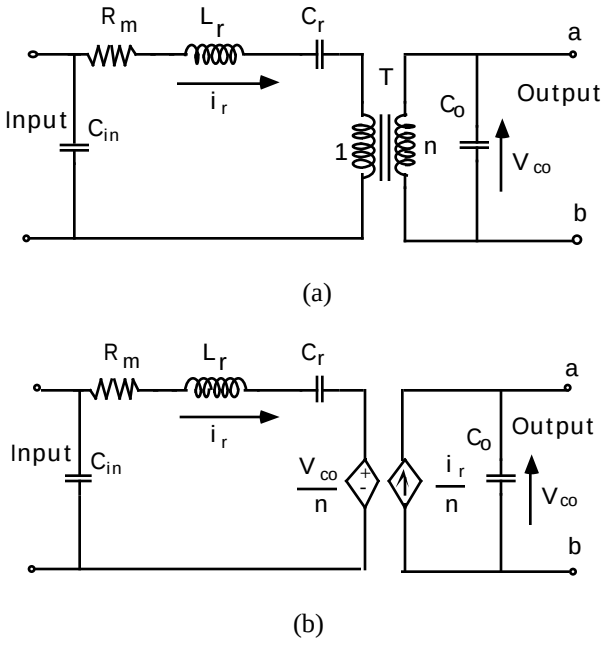

Fig. 1. Equivalent circuits of a piezoelectric transformer (PZT): (a)-conventional model ; (b)-proposed model.

will be reflected to the primary and then blocked by C_r with no effect on the AC signals which are of interest. Hence, the proposed equivalent model seems to be more accurate from the theoretical point of view and a better choice for SPICE simulation.

In typical HV AC-DC application, the PZT will be fed by an AC signal and the output will be rectified to obtain DC. Different inverter topologies can be used at the input side [1-7] but considering the high Q of the PZT device and the fact that operation is normally near the resonant frequency, only the first harmonics of the input voltage will affect the resonant current. The AC output voltage of the PZT can be rectified by any one rectification scheme but considering the primary objective of obtaining a high output voltage, a doubler will be the preferred choice. The voltage doubler rectifier can be one of different topologies (Fig. 2). The simplest one being the non-symmetrical topology with one capacitor C and two diodes (Fig. 2a), although others are possible (Figs. 2b, 2c). In all topologies, R_L is the load resistance.

III. MODEL DEVELOPMENT

Simulated current and voltage waveforms of the rectifier (Fig. 2a), connected to the output of PZT, are shown in Fig. 3. The angle $\vartheta = 2\pi ft$ is normalized time in radians, f is the switching frequency and t is time. Analysis (and simulation) is carried out under the following basic assumptions:

1. Diodes, inductor and capacitors are ideal.
2. Resistance R_m is much lower than the characteristic impedance $\sqrt{\frac{L_r}{C_r}}$ of the $R_mL_rC_r$ branch (Fig. 1) and hence the current i_r of this branch can be approximated by a sinusoidal waveform:

$$i_r = I_{rm}\sin\vartheta \qquad (2)$$

where I_{rm} is the peak of this current.

3. The time constant R_LC is much larger than the switching period 1/f and therefore the ripple of the load voltage V_L can be neglected.

Referring to Fig. 1, Fig. 2a and Fig. 3, the reflected current i_r/n flows through the capacitor C_o of PZT during the non-conduction intervals of both diodes ($\vartheta_0\vartheta_1$ and $\vartheta_2\vartheta_3$) and through the diodes D_1 or D_2 during their conduction intervals ($\vartheta_1\vartheta_2$ and $\vartheta_3\vartheta_4$). Duration of these conduction intervals is defined as θ. The voltage across the capacitor C_o (v_{Co}) is equal to the load voltage V_L during the conduction interval of D_1 (interval $\vartheta_1\vartheta_2$) and is zero during the conduction interval of D_2 (interval $\vartheta_3\vartheta_4$).

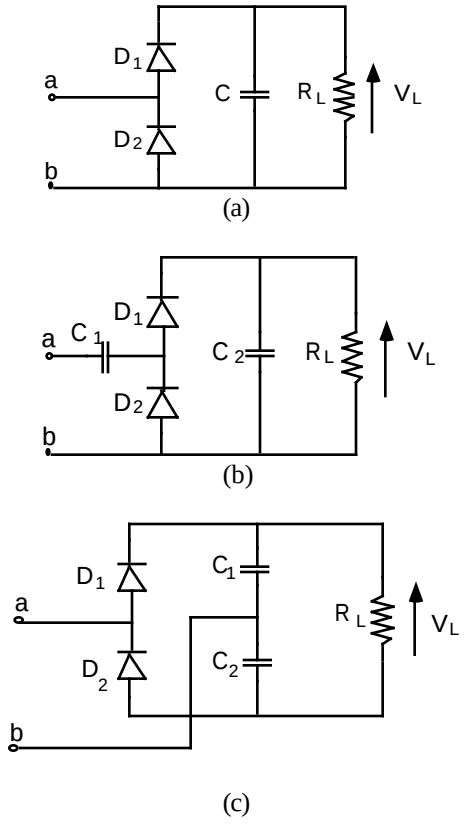

Fig. 2. Possible topologies of voltage-doubler rectifiers:
(a) - non-symmetrical topology with one capacitor;
(b) - non-symmetrical topology with two capacitors;
(c) - symmetrical half-bridge topology.

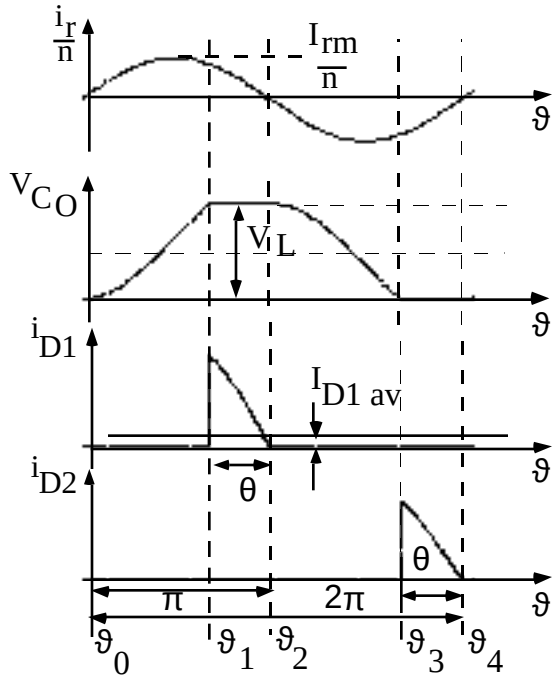

Fig. 3. Simulated current and voltage waveforms of the voltage doubler rectifier (Fig.2a).

The voltage v_{Co} during the nonconduction intervals of both diodes (D_1, D_2) can be divided into distinct operational segments by applying the following initial conditions (Figs. 2a and 3):

at $\vartheta_0=0$ the current i_r/n (eq. (2)) changes its direction and therefore the diode D_2 ceases to conduct, $v_{Co}=0$;

at $\vartheta_1=\pi-\theta$ the capacitor's voltage v_{Co} reaches the load voltage V_L and therefore the diode D_1 begins to conduct;

at $\vartheta_2=\pi$ the current i_r/n (eq. (2)) changes its direction and therefore the diode D_1 ceases to conduct, $v_{Co}=V_L$;

at $\vartheta_3=2\pi-\theta$ the capacitor's voltage v_{Co} reaches zero and therefore the diode D_2 begins to conduct.

Applying (2) along with the above boundary conditions we get for the interval $\vartheta_0\vartheta_1$:

$$v_{Co}=\frac{V_L}{1+\cos\theta}(1-\cos\vartheta) \tag{3}$$

and for the interval $\vartheta_2\vartheta_3$:

$$v_{Co}=\frac{V_L}{1+\cos\theta}(\cos\theta-\cos\vartheta) \tag{4}$$

Taking into account that $v_{Co}=V_L$ or $v_{Co}=0$ in the conducting intervals of the diodes and applying (3) and (4) we obtain the DC component of voltage v_{Co} during the switching period $\vartheta_0\vartheta_4$:

$$(V_{Co})_{dc}=\frac{V_L}{2} \tag{5}$$

Note that the DC component of v_{Co} is blocked by the ceramic material of the PZT. This galvanic isolation effect is emulated by C_r in the proposed equivalent circuit presentation (Fig. 1b).

The same value has the peak of the AC component of the capacitor's C_o voltage v_{Co}:

$$(V_{Co})_{ac\,pk}=\frac{V_L}{2} \tag{6}$$

Hence, the output voltage of the rectifier V_L is twice higher than the peak of the AC component of the capacitor's C_o voltage which can be considered as the input voltage of the rectifier. Therefore this type of rectifier operates as a voltage doubler.

The peak of the reflected current of the $R_mL_rC_r$ branch of the PZT-model (Fig. 1,a) is found from (2) and (3) or (4):

$$\frac{I_{rm}}{n}=\frac{V_L\omega C_o}{1+\cos\theta} \tag{7}$$

where $\omega=2\pi f$.

The current of the load I_L is equal to the average current of the diode D_1:

$$I_L=I_{D1\,av}=\frac{1}{2\pi}\int_{\pi-\theta}^{\pi}\frac{I_{rm}}{n}\sin\vartheta\,d\vartheta=$$

$$=\frac{1}{2\pi}\frac{I_{rm}}{n}(1-\cos\theta) \tag{8}$$

or applying (7):

$$I_L=I_{D1\,av}=\frac{1}{2\pi}V_L\omega C_o\tan^2\left(\frac{\theta}{2}\right) \tag{9}$$

On the other hand:

$$I_L=I_{D1\,av}=\frac{V_L}{R_L} \tag{10}$$

From (9) and (10) we obtain the diodes conduction angle:

$$\theta=2\tan^{-1}\sqrt{\frac{2\pi}{\omega C_o R_L}} \tag{11}$$

It can be shown that all the voltage doubling rectifying topologies of Fig. 2 follow the behavior described above, but in the topologies of Fig. 2b and 2c the DC component of the capacitor's C_o voltage (v_{Co}) is missing. In the case of a full-bridge rectifier circuit with capacitive output filter, but without voltage doubling, the capacitor's C_o voltage (v_{Co})

also includes only an AC component and its peak is V_L; consequently, the value of θ is lower in this rectifier [8]. Based on the above, general equations can be written for the rectifiers with and without voltage doubling :

$$(V_{Co})_{ac\ pk}=\frac{V_L}{a} \tag{12}$$

$$\theta = 2\tan^{-1}\sqrt{\frac{a^2\pi}{2\omega C_o R_L}} \tag{13}$$

where a=1 for the rectifier without voltage doubling and a=2 for the voltage doubler rectifier. Relationship (13) is depicted in Fig. 4.

IV. THE RC EQUIVALENT MODEL

Since the top and bottom of the capacitor's C_o voltage v_{Co} waveform are flat during the conducting intervals of the diodes (Fig. 3), the waveform of this voltage includes high harmonics. In contrast, the waveform of the current i_r of the branch $R_m L_r C_r$ is assumed to be practically a sine wave - due to the high Q of the circuit. Under these conditions only the fundamental harmonic of the voltage v_{Co} affects the output power:

$$P_L=\frac{1}{2}V_{Co(1)m}\frac{I_{rm}}{n}\cos\phi_{(1)} \tag{14}$$

where $V_{Co(1)m}$ is the peak of the fundamental harmonic of the voltage v_{Co} and $\phi_{(1)}$ is its phase angle referred to the instant ϑ_0=0. The values of $V_{Co(1)m}$ and $\phi_{(1)}$ are found from the following equations:

$$V_{Co(1)m}= k_{v(1)}(V_{Co})_{ac\ pk} \tag{15}$$

$$\phi_{(1)}= \tan^{-1}\left(\frac{a_{v(1)}}{b_{v(1)}}\right) \tag{16}$$

where $k_{v(1)}$ is the voltage waveform coefficient [8]:

$$k_{v(1)} = \sqrt{a_{v(1)}^2 + b_{v(1)}^2} \tag{17}$$

and

$$a_{v(1)} = -\frac{2}{\pi}\left[\frac{\pi-\theta+\frac{1}{2}\sin(2\theta)}{1+\cos\theta}\right] \tag{18}$$

$$b_{v(1)} = \frac{2}{\pi}(1-\cos\theta) \tag{19}$$

Note that $\phi_{(1)}<0$ because $a_{v(1)}<0$. Eqs. (16)-(19) show that $\phi_{(1)}$ and $k_{v(1)}$ are uniquely defined by θ. Taking into account (13) we find that $\phi_{(1)}$ and $k_{v(1)}$ are functions of $\frac{\omega C_o R_L}{a^2}$. These relationships are depicted in Fig. 4.

Considering the fact that $\phi_{(1)}<0$, the network including the capacitor C_o, output rectifier and load can be represented by a R_e-C_e parallel equivalent circuit (Fig. 5a). The equivalent load resistance R_e was found from the relationship:

$$P_L=\frac{V_{Co(1)m}^2}{2R_e}=\frac{V_L^2}{R_L} \tag{20}$$

Applying (20), (15) and (12):

$$R_e = \frac{k_{v(1)}^2\ R_L}{2a^2} \tag{21}$$

The equivalent capacitance C_e was found from Fig. 5b to be:

$$C_e = \frac{\tan|\phi_{(1)}|}{\omega R_e} \tag{22}$$

Note that C_e includes two components: the real capacitance C_o and an additional capacitance C_{ad}:

$$C_e=C_o+C_{ad} \tag{23}$$

From (22) and (23):

$$C_{ad}=\frac{\tan|\phi_{(1)}|}{\omega R_e}-C_o \tag{24}$$

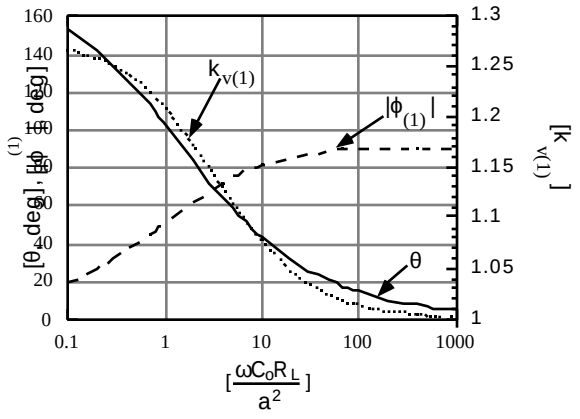

Fig. 4. Rectifier conduction angle θ, the phase angle $\phi_{(1)}$ and the voltage waveform coefficient $k_{v(1)}$ as functions of the load coefficient $\frac{\omega C_o R_L}{a^2}$.

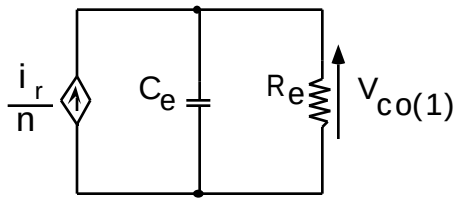

(a)

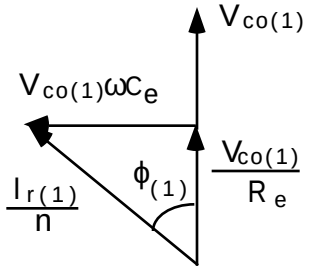

(b)

Fig. 5. Equivalent R_e - C_e circuit replacing the network fed by the current $\frac{I_r}{n}$ (a) topology ; (b) vector diagram.

The relationships $\frac{a^2R_e}{R_L}$ and $\frac{C_{ad}}{C_o}$ as a function of $\frac{\omega C_o R_L}{a^2}$, calculated by (13), (16)-(19), (21) and (24), are depicted on Fig 6. Note that $\frac{C_{ad}}{C_o}$ is small when $\frac{\omega C_o R_L}{a^2}$ >10.

The presented approach can be considered as a modification of the approximate analysis of steady state processes in voltage-fed parallel and series-parallel resonant converters with capacitive output filter [8]. The new approach is simpler: since capacitance C_o is included in the R_e-C_e equivalent circuit it is not necessary now to obtain the phase angle between the first harmonics of the capacitor's C_o voltage and the input current of the rectifier. Additional capacitance C_{ad} obtained from (24) is equal to the value C_e given in [8].

Applying the equivalent resistance R_e and the equivalent capacitance C_e, the system including the PZT and the output rectifier can be represented by the equivalent circuit of Fig. 7 (resistance R_m of the PZT is neglected in Fig. 7). $V_{in(1)m}$ is the peak of the first harmonic of the input voltage.

The expression of the (ac output)/(ac input) voltage ratio

$$k_{21} = \frac{V_{Co(1)m}}{nV_{in(1)m}} \qquad (25)$$

can be found by analyzing this equivalent circuit:

$$k_{21} = \frac{1}{\sqrt{[1+\frac{n^2C_e}{C_r} - \omega^2 L_r n^2 C_e]^2 + (\omega L_r - \frac{1}{\omega C_r})^2 \frac{n^2}{R_e^2}}} \qquad (26)$$

or:

$$k_{21} = \frac{1}{\sqrt{\{1-\frac{n^2C_e}{C_r}[(\frac{\omega}{\omega_r})^2 -1]\}^2 + \{\frac{n^2C_e}{C_r}[(\frac{\omega}{\omega_r})^2 -1]\frac{1}{\tan\phi_{(1)}}\}^2}} \qquad (27)$$

where $\omega_r = 2\pi f_r$.

Note that k_{21}=1 when $\omega = \omega_r$. The impedance of the series circuit L_rC_r is zero in this case and therefore the AC input voltage imposed across the parallel circuit $n^2C_e \| R_e/n^2$. That is why the load voltage (denoted in this case as $(V_L)\omega_r$) is practical independent of the load coefficient $\frac{\omega C_o R_L}{a^2}$.

In the case $\omega > \omega_r$ the series circuit L_rC_r is inductive and therefore the voltage across the parallel circuit $n^2C_e \| R_e/n^2$ can be higher than the AC input voltage: k_{21}>1. The expression of the frequency ratio $(\frac{\omega}{\omega_r})_{max}$ corresponding to the maximum value of k_{21} ($(k_{21})_{max}$) was found from (27) under the assumption that the values $\phi_{(1)}$ and C_e are constant and independent of the frequency ratio $\frac{\omega}{\omega_r}$:

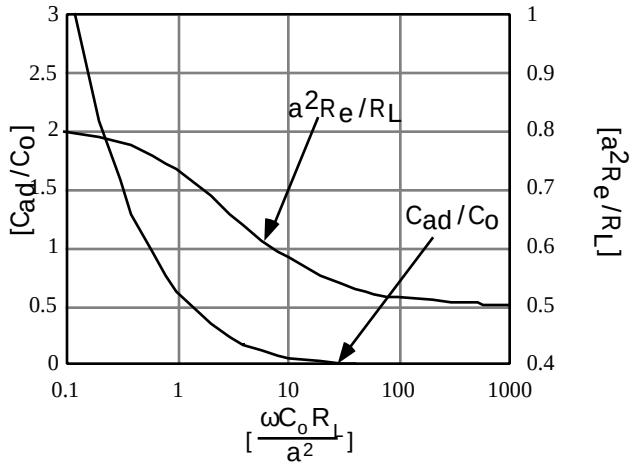

Fig. 6. Equivalent load resistance R_e (pu) and apparent additional capacitance C_{ad} (pu) as functions of the load coefficient $\frac{\omega C_o R_L}{a^2}$.

.

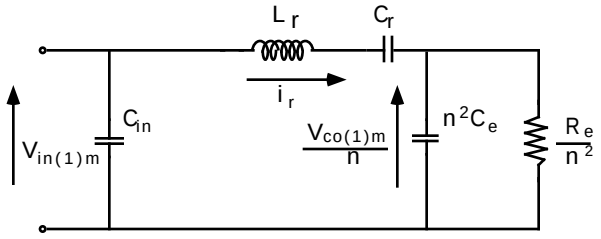

Fig. 7. AC equivalent circuit of the system: PZT - output rectifier

$$\left(\frac{\omega}{\omega_r}\right)_{max} = \sqrt{1+\frac{C_r}{n^2 C_e}\sin^2\phi(1)} \qquad (28)$$

The above equation implies:

$$\left(\frac{\omega}{\omega_r}\right)_{max} = \sqrt{1+\frac{C_r}{n^2 C_o}\,\frac{C_o}{C_e}\sin^2\phi(1)} < \sqrt{1+\frac{C_r}{n^2 C_o}} \qquad (29)$$

Note that $\omega_r\sqrt{1+\frac{C_r}{n^2 C_o}}$ is the resonant frequency of the equivalent circuit (Fig. 7) under no load condition ($R_e=\infty$) and is therefore the highest resonant frequency of the circuit. On the other hand,

$$\left(\frac{\omega}{\omega_r}\right)_{max} > 1 \qquad (30)$$

Hence

$$1 < \left(\frac{\omega}{\omega_r}\right)_{max} < \sqrt{1+\frac{C_r}{n^2 C_o}} \qquad (31)$$

Inserting in (31) the parameter values of the experimental PZT (as measured by our group) we obtain:

$$1 < \left(\frac{\omega}{\omega_r}\right)_{max} < 1.1 \qquad (32)$$

Figs. 4 and 6 show that such a small frequency range causes insignificant changes in the values of $\phi(1)$ and C_{ad} which is the variable part of C_e (23). Therefore our assumption about C_e and $\phi(1)$ in dependence on the frequency ratio $\frac{\omega}{\omega_r}$ is a good approximation to obtain $\left(\frac{\omega}{\omega_r}\right)_{max}$ from (27).

Inserting (28) into (27) we obtain the maximum value of k_{21} ($(k_{21})_{max}$):

$$(k_{21})_{max} = \frac{1}{\cos\phi(1)} \qquad (33)$$

The expression of the normalized maximum value of the load voltage

$$V_{Lmax}^{*} = \frac{V_{Lmax}}{V_{in(1)m}} \qquad (34)$$

is found from (12), (15), (25) and (33) under the assumption that $k_{v(1)}$ is independent of $\frac{\omega}{\omega_r}$:

$$V_{Lmax}^{*} = \frac{a\,n\,(k_{21})_{max}}{k_{v(1)}} = \frac{a\,n}{k_{v(1)}\cos\phi(1)} \qquad (35)$$

V. EXPERIMENTAL

The experimental circuit is shown in Fig. 8. Philips PZT (PXE43, 48x8x2 mm) was fed through a coupling capacitor C_{se} from the output of a half-bridge high frequency inverter. The parameters of the PZT (Fig. 1a) were [9]:

C_{in}=735 pF, C_o=5.5 pF, C_r=24.5 pF, L_r= 201 mH, R_m= 63 Ω and n=5.6.

The frequency range was 65 - 80kHz. The load resistance R_L was changed from 395 kΩ to 19.2MΩ. Relationships between the load voltage V_L and R_L were measured in two cases (Fig. 9):

1) when the operating frequency f was equal to the resonant frequency f_r. For the PZT under study, f_r=71.72kHz;
2) when f was corrected so as to get maximum output voltage: $V_L=V_{Lmax}$.

The rms input voltage of PZT $V_{in\ rms}$ was held constant: 62V in the first case and 52.5V in the second case.

The deviation of the model prediction from the experimental results (Fig. 9) was found to be smaller than 13%.

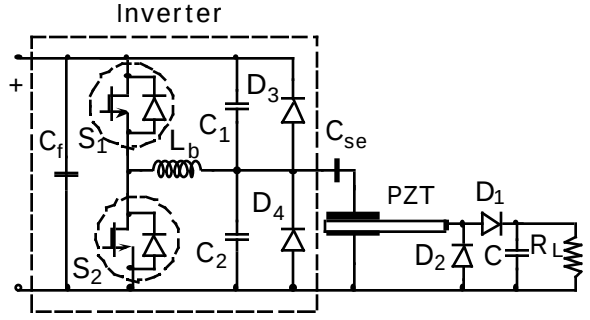

Fig. 8. The experimental circuit.

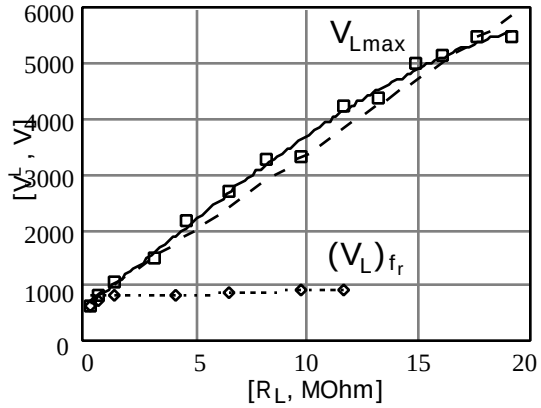

Fig. 9. DC output voltage as a function of the load resistance R_L. Experimental data (points) and theoretical model (broken lines). $(V_L)_{f_r}$ - voltage corresponding to the resonant frequency f_r; V_{Lmax} - maximum output voltage reached by frequency adjustment.

VI. DISCUSSION AND CONCLUSIONS

The system under study is of a high order and consequently, precise analytical relationships are difficult if not impossible to derive. The proposed approximate derivation hinges on the specific characteristics of the physical HV PZT. In such a transformer the apparent turns ratio factor (n) is relatively large. Hence, even though the output capacitance (C_o) is small the ratio $\frac{C_r}{n^2 C_o}$ is relatively small (0.1 in the experimental PZT). As a result, the expected range for $(\frac{\omega}{\omega_r})_{max}$ per (31) is small. For such a narrow frequency window, $\phi_{(1)}$ and C_e can be assumed to be approximately constant (Fig. 6) which makes possible taking the derivative of (27) to find $(\frac{\omega}{\omega_r})_{max}$. If the frequency window for $(\frac{\omega}{\omega_r})_{max}$ of a given PZT is not narrow, the approximate equations derived here may not apply. For the experimental PZT, the proposed modeling and analysis of the AC-DC HV circuit that include voltage doubler was shown to agree well with experimental measurements.

When applicable, the proposed R-C model offers a simple way to analyze the behavior of the AC-DC HV PZT circuit. Furthermore, since the resulting equivalent circuit is SPICE compatible it can be used to examine by simulation the behavior of the PZT-rectifier assembly by running frequency domain (AC) analysis, which is much faster than time domain simulation (TRAN).

REFERENCES

[1] C. Y. Lin and F. C. Lee, "Development of a piezoelectric transformer converter", *VPEC Seminar Proceedings*, Blacksburg, Virginia, U.S.A., 1993, pp. 79-85.

[2] "Piezoelectric transformers". *Philips Components. Application note. Philips Magnetic Products.* Date of release: 2/97.

[3] M. Shoyama, K. Horikoshi, T. Ninomiya, T. Zaitsu, Y. Sasaki, "Operation analysis of the push-pull piezoelectric inverter", *IEEE APEC'97 Record*, pp. 573-578.

[4] M. Shoyama, K. Horikoshi, T. Ninomiya, T. Zaitsu, Y. Sasaki, "Steady-state characteristics of the push-pull piezoelectric inverter", *IEEE PESC'97 Record*, pp. 715-721.

[5] H. Kakehashi, T. Hidaka, T. Ninomiya, M. Shoyama, H. Ogasawara, Y. Ohta, "Electronic ballast using piezoelectric transformers for fluorescent lamps", *IEEE PESC'98 Record*, pp. 29-35.

[6] T. Yamane, S. Hamamura, T. Zaitsu, T. Ninomiya, M. Shoyama, Y. Fuda, "Efficiency improvement of piezoelectric-transformer dc-dc converter", *IEEE PESC'98 Record*, pp. 1255-1261.

[7] A. M. Flynn and S. R. Sanders, " Fundamental limits on energy transfer and circuit considerations for piezoelectric transformers", *IEEE PESC'98 Record*, pp. 1463-1471.

[8] G. Ivensky, A. Kats, S. Ben-Yaakov, "A RC load model of parallel and series-parallel resonant dc-dc converters with capacitive output filter", *IEEE Trans. on Power Electronics*, vol. 14, no. 3, 1999, pp.958-964 .

[9] Philips, Eindhoven, The Netherlands. Private communication.